

Observation of Strong Nonreciprocal Thermal Emission

Zhenong Zhang^{1†}, Alireza Kalantari Dehaghi^{1†}, Prमित Ghosh¹, Linxiao Zhu^{1*}

¹Department of Mechanical Engineering, The Pennsylvania State University, University Park,
PA 16802, United States.

†These authors contributed equally to this work.

*Corresponding author. Email: lqz5242@psu.edu

Abstract

The Kirchhoff's law of thermal radiation stating the equivalence of emissivity and absorptivity at the same wavelength, angle, and polarization, has completely constrained emission and absorption processes. Achieving strong nonreciprocal emission points to fundamental advances for applications such as energy harvesting, heat transfer, and sensing, but strong nonreciprocal thermal emission has not been experimentally realized. Here, we observe strong nonreciprocal thermal emission using a custom-designed angle-resolved magnetic thermal emission spectroscopy and an epitaxially-transferred gradient-doped metamaterial. We show that under magnetic field, the metamaterial strongly breaks the Kirchhoff's law, with a difference between emissivity and absorptivity at the same wavelength and angle reaching as high as 0.43. Significant nonreciprocal emission persists over broad spectral and angular ranges. The demonstration of strong nonreciprocal thermal emission and the approach can be useful for systematic exploration of nonreciprocal thermal photonics for thermal management, infrared camouflage, and energy conversion.

The Kirchhoff's law of thermal radiation states that, for an arbitrary object, the emissivity must equal the absorptivity, at the same wavelength, angle, and polarization [1-3]. Such reciprocal relation between emission and absorption has played a foundational role in understanding and controlling emission [4-8]. Breaking the reciprocal relation between emission and absorption can not only provide a way for separately controlling emission and absorption, but also point to energy harvesting at thermodynamic limits such as in solar cells [9,10], thermophotovoltaics [11,12] and harvesting outgoing radiation [11,13], advanced heat flux control [14] and communication [15].

The Kirchhoff's law of thermal radiation is not required by thermodynamics, but rather is the consequence of Lorentz reciprocity [16,17]. It has been pointed out that nonreciprocal emission and absorption can be achieved by breaking the Lorentz reciprocity [18-22], leading to unequal emissivity $e(\lambda, \theta)$ and absorptivity $\alpha(\lambda, \theta)$ with $e(\lambda, \theta) \neq \alpha(\lambda, \theta)$, as schematically shown in Fig. 1(a). While there have been great advances in the theory of nonreciprocal emission and absorption in magneto-optical materials [23-25] and magnetic Weyl semimetals [26-28], experimental demonstration of nonreciprocal emission is lacking and the achieved nonreciprocity defined as the difference between emissivity and absorptivity is small. Recent experiments measured nonreciprocal thermal emission from heated InAs-based emitter under magnetic field [29,30]. In Ref. [29], a grating-coupled InAs substrate was used to achieve a nonreciprocity about 0.22 around a wavelength. In Ref. [30], an InAs multilayer was used to achieve a nonreciprocity about 0.12. Though strong nonreciprocal emission is necessary for achieving energy conversion at thermodynamic limits and nonreciprocal heat flux control [25], demonstration of strong nonreciprocal thermal emission has been elusive, owing to the challenges of creating high-quality thin-film structures, and measuring emission over broad spectral and angular ranges while providing a substantial magnetic field. We note that nonreciprocal absorption was demonstrated at room temperature by measuring bi-directional reflectance [31-33], but emission of the sample was not measured.

Here we report an experimental observation of strong nonreciprocal thermal emission in an infrared metamaterial using a custom-designed angle-resolved magnetic thermal emission spectroscopy. We achieve a difference between emissivity and absorptivity at the same wavelength and angle up to 0.43 on a gradient-doped epsilon-near-zero $\text{In}_{0.53}\text{Ga}_{0.47}\text{As}$ (hereafter referred to as InGaAs) metamaterial atop gold. The metamaterial also shows significant nonreciprocal emission over broad spectral and angular ranges. It is noteworthy that we transferred the micrometer-scale-

thick epitaxial sample to a foreign substrate, enabling its integration with devices for nonreciprocal-based applications. Beyond nonreciprocal emission, our findings also show that strong dynamic control of thermal emission can be achieved using magnetic field, in addition to electrical [34,35] and electrochemical approaches [36].

We designed and fabricated a gradient-doped epsilon-near-zero (ENZ) metamaterial, consisting of five 440-nm-thick electron-doped InGaAs layers atop 100-nm Au, as schematically shown in Fig. 1(b) with a scanning electron microscope cross-section. Details of sample fabrication are described in the Supplemental Material [37] and Fig. S1 in [37]. The doping concentration increases as the depth increases, with concentrations denoted in Fig. 1(b). A thin film can support Berreman mode [44] at wavelengths where the permittivity is near zero. The gradient doping allows deeper layers to reach the ENZ condition at progressively shorter wavelengths, creating cascading of Berreman modes. We transferred the epitaxially grown InGaAs layers to a Si substrate using thermocompression bonding [45,46]. Such epitaxial transfer, by allowing for using low-loss noble metal as reflector, can reduce parasitic reciprocal thermal emission at short wavelengths, when compared to using doped semiconductor substrates [29-32]. Further, transferring the epitaxial thin film to a foreign substrate allows for its integration with devices for nonreciprocal-based applications.

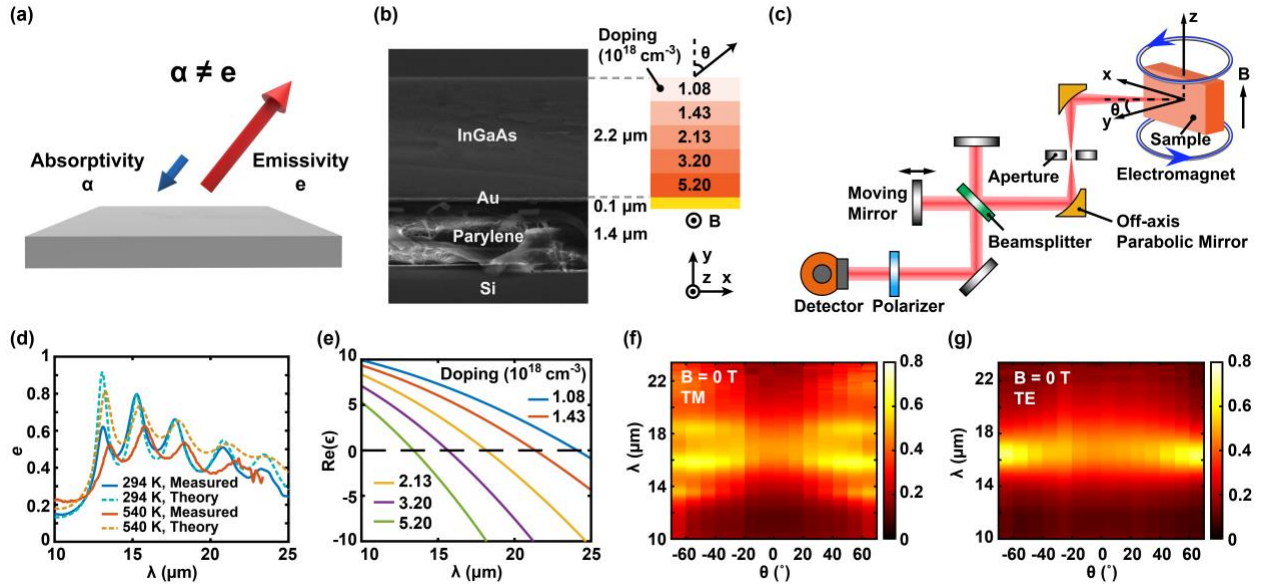


FIG. 1. Sample and experimental set-up. (a) Schematic of nonreciprocal emission and absorption. (b) Scanning electron microscope image of an InGaAs multilayer. It consists of five 440-nm-thick layers of gradient-doped InGaAs on top of 100-nm-thick gold. The doping concentration increases with the depth. (c) Schematic of the angle-resolved magnetic thermal emission spectroscopy setup.

(d) Emissivities of the sample at TM polarization and 65° , measured at 540 K and obtained at room temperature (solid lines). Modeled emissivities at the corresponding temperatures are shown in dashed lines. (e) Spectra of real part of the permittivity ϵ of each InGaAs layer at 540 K. (f-g) Measured emissivities of sample at 540 K, for (f) TM and (g) TE polarizations. In (d-g), there is no external magnetic field.

The relative permittivity of InGaAs in the presence of a magnetic field $\vec{B} = B\hat{z}$, is:

$$\bar{\epsilon} = \epsilon_\infty \bar{I} - \frac{\omega_p^2}{(\omega - i\Gamma)^2 - \omega_c^2} \begin{bmatrix} 1 - i\frac{\Gamma}{\omega} & i\frac{\omega_c}{\omega} & 0 \\ -i\frac{\omega_c}{\omega} & 1 - i\frac{\Gamma}{\omega} & 0 \\ 0 & 0 & \frac{(\omega - i\Gamma)^2 - \omega_c^2}{\omega(\omega - i\Gamma)} \end{bmatrix}.$$

Here, ϵ_∞ is the relative permittivity of undoped InGaAs, $\omega_p = \sqrt{\frac{nq^2}{m^*\epsilon_0}}$ is the plasma frequency, Γ is the relaxation rate, $\omega_c = qB/m^*$ is the cyclotron frequency, m^* is the electron effective mass, q is the charge of a proton, and n is the electron concentration. Details of permittivity model are described in Ref. [37]. In the magnetic field, due to free-carrier magneto-optical effect, the permittivity tensor becomes asymmetric, breaking the Lorentz reciprocity. We consider InGaAs because it has low electron effective mass [47] leading to high cyclotron frequency and thus strong nonreciprocal effect, and it can be epitaxially transferred to a foreign substrate for device integration [45].

To overcome the challenge of measuring the thermal emission of a sample at various angles in a substantial magnetic field, we custom-designed an angle-resolved magnetic thermal emission spectroscopy set-up as schematically shown in Fig. 1(c). The set-up integrates a cryostat, a superconducting electromagnet, and a Fourier-transform infrared spectrophotometer (see details of measurement in Ref. [37]). The sample is mounted on a temperature-controlled, fully-rotatable sample holder in a high vacuum ($<1 \times 10^{-6}$ Torr) in the cryostat. The electromagnet provides magnetic field up to ± 5 T, allowing for fully exploring magnetic control of nonreciprocal emission. The thermal radiation of the sample is reflected off two off-axis parabolic mirrors, through an interferometer and an infrared linear polarizer, and collected by a mercury-cadmium telluride (MCT) detector. We measure signal I_S from the sample heated to temperature T_S , a reference signal I_R from a high-emissivity coating heated to T_S , and a background signal I_{BG} from a high-emissivity coating at the ambient temperature ~ 294 K. The spectral, angular emissivity of the sample e_ζ is determined as:

$$e_S(\lambda, \theta, B, T_S) = e_R(\lambda) \cdot \frac{I_S(\lambda, \theta, B, T_S) - I_{BG}(\lambda, 294 \text{ K})}{I_R(\lambda, T_S) - I_{BG}(\lambda, 294 \text{ K})},$$

where e_R is the emissivity of the high-emissivity coating. Details of the emissivity and measurement of the high-emissivity coating are described in Ref. [37] and Fig. S2. On one hand, for a specular sample, thermodynamics requires that the emissivity equals the absorptivity at the opposite angle, leading to $e(\theta, -B) = \alpha(-\theta, -B)$ [23]. On the other hand, due to the 2-fold rotational symmetry of the sample, after rotating both the angle and the magnetic field around the normal direction y by 180° , the absorptivity must remain unchanged, leading to $\alpha(-\theta, -B) = \alpha(\theta, B)$. Using both thermodynamics and rotational symmetry, we have $\alpha(\theta, B) = e(\theta, -B)$ for our sample [48,49]. Therefore, in the experiment, we will determine absorptivity $\alpha(\theta, B)$, by measuring the emissivity at the same angle but reversed magnetic field $e(\theta, -B)$. The nonreciprocity [$e(\theta, B) - \alpha(\theta, B)$], is equivalent to the contrast $\Delta e = e(\theta, B) - e(\theta, -B)$ between the emissivity at B and that at $-B$.

We start by investigating emission at zero magnetic field. At 65° and TM polarization, a reflectance-based measurement at room temperature shows five emissivity peaks at wavelengths between 13 and 25 μm , as shown in Fig. 1(d) (see details of measurement in Ref. [37] and Fig. S3 for all angles and both polarizations). Each emissivity peak corresponds to the ENZ wavelength of an individual InGaAs layer, as shown in Fig. 1(e). Using the angle-resolved magnetic thermal emission spectroscopy, at the same angle and polarization, we observe a redshift of the emissivity peaks for sample at 540 K [Fig. 1(d)]. The redshift can be explained largely by the increasing refractive index as the temperature rises [42] (see details in Ref. [37] and Fig. S4). For the topmost InGaAs layer with the lowest doping, at room temperature, its ENZ wavelength corresponding to strong emission is at $\sim 23.3 \mu\text{m}$. At 540 K, the ENZ wavelength and accordingly the emissivity peak will shift to longer wavelength outside the wavelength range of the detector. The measured emissivities agree well with modeling results [dashed lines, Fig. 1(d)] based on fluctuational electrodynamics [23,50] (see Ref. [37] for the modeling of permittivity). The emissivity at zero magnetic field exhibits left-right symmetry at both TM and TE polarizations, that is $\epsilon(\theta, B) = \epsilon(-\theta, B)$, as shown in Figs. 1(f-g) at 540 K. For the specular sample, as $\epsilon(-\theta, B) = \alpha(\theta, B)$ [23], the mirror symmetry of emissivity signifies reciprocal emission and absorption.

To break the reciprocity between emission and absorption, we apply $\pm 5 \text{ T}$ magnetic field to the sample at 540 K, and measure the sample's emissivity using the angle-resolved magnetic

thermal emission spectroscopy. In a magnetic field, the emissivity in TM polarization becomes asymmetric, as shown in Figs. 2(a-b). At 5 T magnetic field, there is strong broadband emission towards positive angles [Fig. 2(a)]. There are four emissivity peaks corresponding to Berreman mode of each InGaAs layer, covering a broad spectral range from 13 μm to 23 μm . In contrast, the emissivity is much weaker towards negative angles. However, at -5 T magnetic field, the emissivity shows opposite angular dependence compared to that at 5 T [Fig. 2(b)]: the emissivity is high towards negative angles, but weak towards positive angles. As a result, over a broad spectral range from 13 to 23 μm , there is strong contrast Δe between the emissivity at 5 T and that at -5 T, which is equal to the nonreciprocity $[e(5T) - \alpha(5T)]$, shown in Fig. 2(c). Moreover, Fig. 2(d) shows that there is nonreciprocal emission over a broad angular range. At the wavelength of 21.6 μm and 5 T, nonreciprocity is 0.14 at 15° , reaches the maximum of 0.43 at 55° , and remains >0.4 at 65° . Our experiment for the first time realizes strong nonreciprocal emission, with nonreciprocity as high as 0.43, which is much higher than the 0.22 reported in Ref. [29], and the 0.12 reported in Ref. [30]. Further, as thermal radiation contains broad spectral and angular ranges, the achieved nonreciprocity with broad spectral and angular ranges provides strong nonreciprocal overall radiative heat flux.

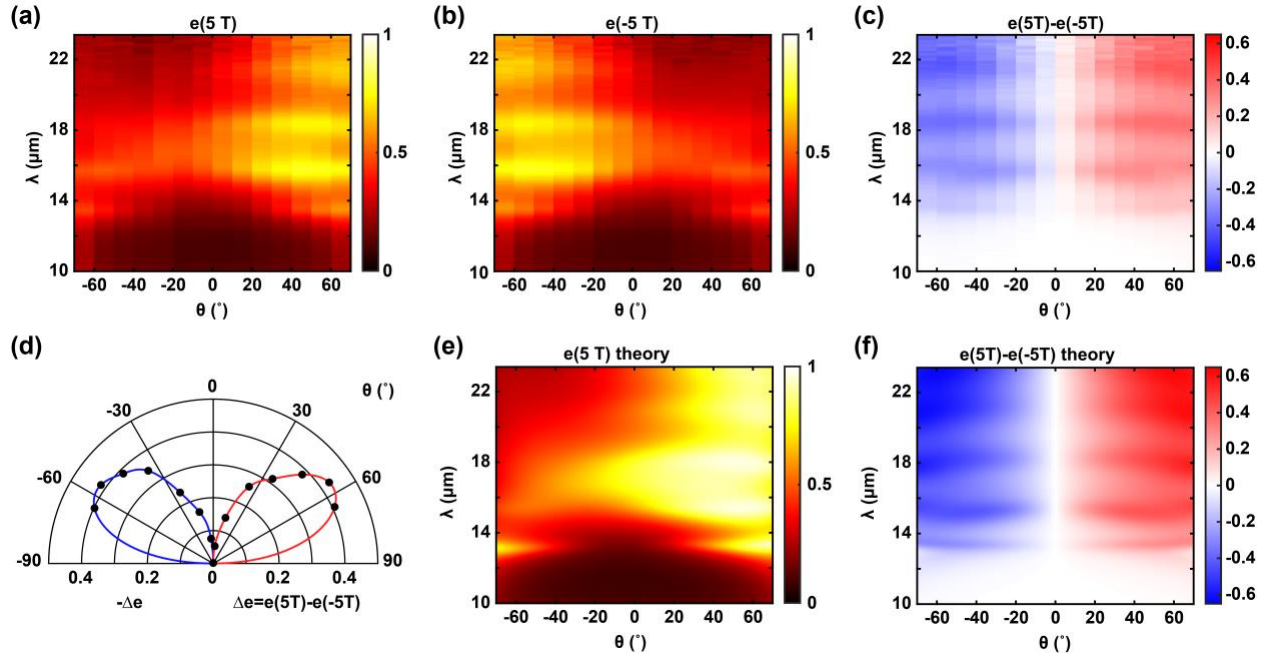


FIG. 2. Spectral and angular response of nonreciprocal emission. (a) Measured spectral, angular emissivity of the sample at 5 T magnetic field. (b) Measured spectral, angular emissivity at -5 T, which is equivalent to spectral, angular absorptivity at 5 T. (c) Difference between measured emissivity at 5 T and that at -5 T, which is equivalent to nonreciprocity. (d) Angular dependence of the contrast between the measured emissivity at 5 T and that at -5 T, at 21.6 μm wavelength.

(e) Modeled emissivity at 5 T. (f) Modeled difference between emissivity at 5 T and that at -5 T. TM polarization is considered throughout (a-f).

To compare with the measurements, we model the emissivity within the framework of fluctuational electrodynamics [23,50]. Figures 2(e-f) show the modeled emissivity at 5 T, and the emissivity contrast between the cases of 5 T and -5 T. The modeled spectra agree well with the measurements in Figs. 2(a) and 2(c), by accounting for increased relaxation rates at elevated temperature [40] (see permittivity model in the Ref. [37]).

As nonreciprocal emission is enabled by magnetic field, a key question in this context is how the nonreciprocal emission depends on the magnetic field. To answer this we performed measurements at various magnetic fields (-5 T to 5 T with increment of 1 T) for TM polarizations. Data obtained from these measurements are shown at Figs. 3(a) and 3(d) for 55° and -55°, respectively (see Figs. S5-S16 in [37] for measurements at other angles). It can be seen that at 55°, as the magnetic field increases from -5 T to 5 T, the emissivity is enhanced over a broad spectral range, especially at the peaks corresponding to the ENZ wavelengths of InGaAs layers. The strong variation of the emissivity as the magnetic field changes results in a substantial difference between emissivity at B and that at $-B$ for 55°, which equals nonreciprocity, as shown in Fig. 3(b). The nonreciprocity is stronger at longer wavelengths, maximizing at the resonance wavelength corresponding to second topmost InGaAs layer. We note that the resonance wavelength of the topmost InGaAs layer at 540 K falls outside the wavelength range of the MCT detector used in the measurement. The nonreciprocity increases as the magnetic field increases. Figure 3(c) shows the measured the emissivity contrast Δe between B and $-B$, at 55° and wavelengths corresponding to the resonance of each layer. It can be seen that, at magnetic fields within 3 T, the nonreciprocity scales linearly as the magnetic field. However, at magnetic field larger than 3 T, the increase of the nonreciprocity becomes sub-linear, especially at the two longer resonant wavelengths [Fig. 3(c)].

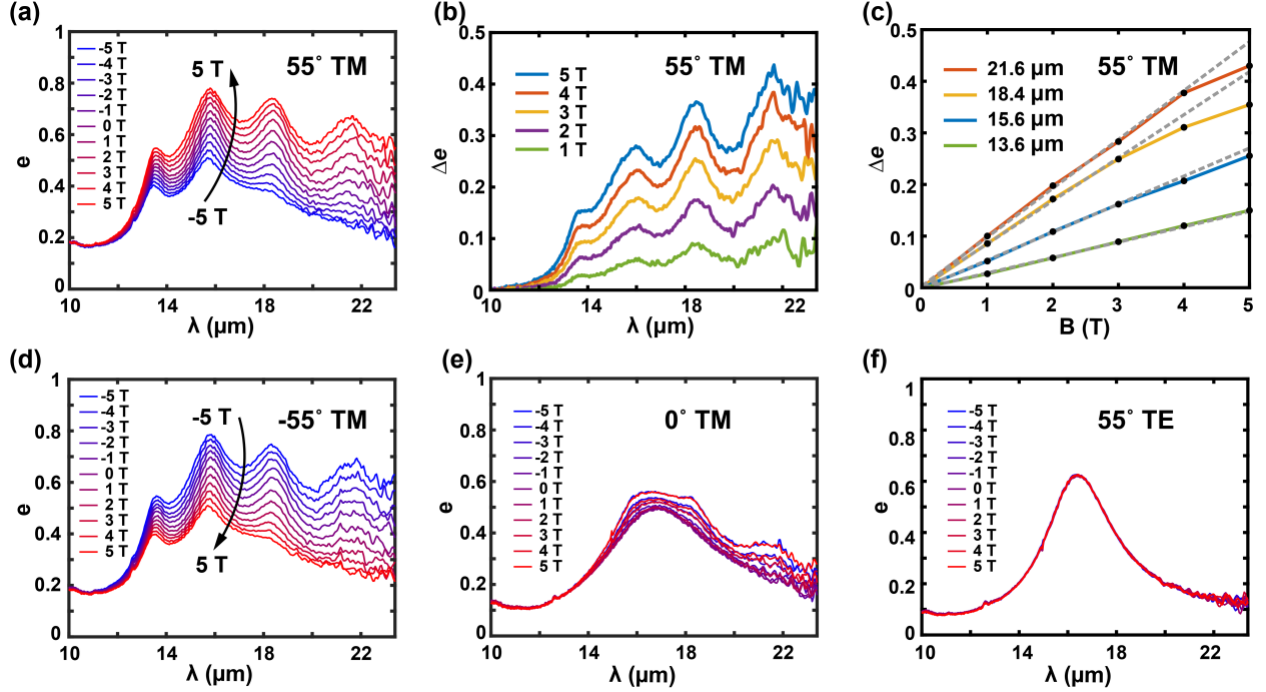


FIG. 3. Magnetic control of nonreciprocal emissivity. (a) Measured TM-polarized emissivity at 55° at varying magnetic fields. (b) The contrast between the measured emissivity at B and the emissivity at $-B$, as a function of wavelength, for varying magnetic fields at 55° and TM polarization. (c) The magnetic field dependence of emissivity contrast, at 55° and resonant wavelengths. The dashed lines denote linear fitting at $B \leq 3$ T. (d-f) Measured emissivity for varying magnetic fields, at (d) -55° and TM polarization, (e) 0° and TM polarization, and (f) 55° and TE polarization.

The magnetic dependence of TM-polarized emissivity at -55° shows opposite trend compared to that at 55° [Fig. 3(d)]. At -55° , as the magnetic field varies from -5 T to 5 T, the TM-polarized emissivity decreases. At 0° , the TM-polarized emissivity slightly increases as the magnitude of magnetic field rises from 0 T to 5 T, as shown in Fig. 3(e). Such dependence on magnetic field results from the fact that at 0° , the electromagnetic response at TM polarization is determined by $\epsilon_{xx} = \epsilon_\infty - \frac{\omega_p^2(\omega - i\Gamma)}{\omega[(\omega - i\Gamma)^2 - \omega_c^2]}$, which slightly depends on the magnetic field through the cyclotron frequency ω_c . In contrast to oblique angles, at 0° , the TM-polarized emissivity remains the same between B and $-B$, leading to reciprocal emission. Therefore, for our sample, achieving nonreciprocal emission in TM polarization requires both nonzero external magnetic field and oblique angle.

We investigate the dependence of TE-polarized emissivity on the magnetic field. The TE-polarized emissivity at 55° remains completely unchanged as magnetic field changes, as shown in Fig. 3(f) (see Fig. S17 in [37] for measured TE-polarized emissivity at 65°). The independence of

TE-polarized emissivity from magnetic field is due to the fact that electromagnetic response in the TE polarization is determined by ϵ_{zz} which is not influenced by the magnetic field along z -direction.

To gain further insights into nonreciprocal emission, and to understand the effects of angle and magnetic field, we examined detailed measurement results. Figures 4(a-d) show the measured emissivity in the B - θ plane at ENZ wavelength of each InGaAs layer. The measured emissivity peaks at very positive B and θ , as well as at very negative B and θ . The emissivity remains unchanged after flipping both the angle and magnetic field, that is $e(\theta, B) = e(-\theta, -B)$, which is consistent with the 2-fold rotational symmetry of the sample around y axis.

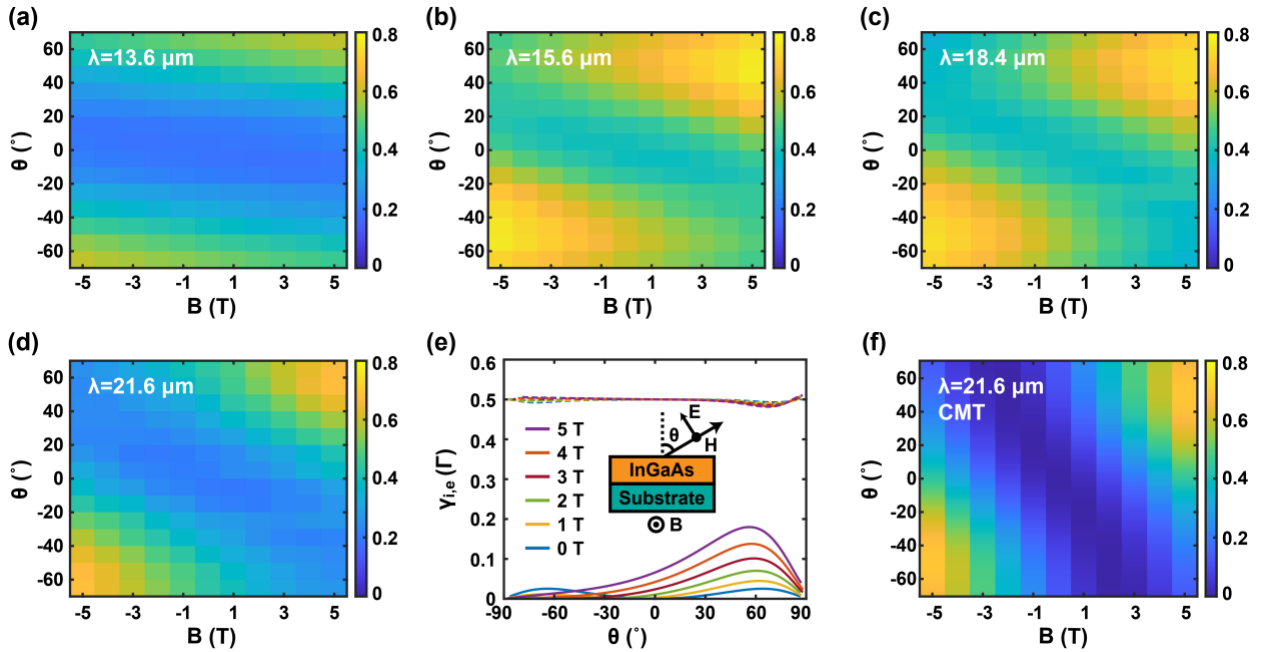


FIG. 4. Emissivity as a function of magnetic field and angle. (a-d) Measured emissivity in $B - \theta$ plane, at wavelengths corresponding to Berreman mode of each InGaAs layer, including (a) $13.6 \mu\text{m}$, (b) $15.6 \mu\text{m}$, (c) $18.4 \mu\text{m}$, and (d) $21.6 \mu\text{m}$. (e) Intrinsic decay rate (dashed lines) and external decay rate (solid lines) for 440-nm-InGaAs atop a substrate at different angles and magnetic fields at TM polarization. The decay rates are normalized by the material relaxation rate Γ . The calculation assumes that InGaAs has an electron concentration of $1.43 \times 10^{18} \text{ cm}^{-3}$, the substrate has a relative permittivity of -4 , and the temperature is 540 K. (f) Modeled emissivity at $21.6 \mu\text{m}$ using coupled mode theory (CMT).

To understand the intricate dependence of emissivity on magnetic field and angle, we perform analysis using temporal coupled mode theory (CMT) [51,52]. The peak emissivity due to a resonant mode can be expressed as $4\gamma_i\gamma_e/(\gamma_i + \gamma_e)^2$, where γ_i and γ_e are the intrinsic and the external modal decay rates, respectively. Unity emissivity can be reached when the intrinsic and the external decay rates match each other. For a 440-nm-thick InGaAs layer with magnetic field

applied in the Voigt geometry, the decay rates at TM polarization are shown in Fig. 4(e). Details of calculation are described in Ref. [37]. While γ_i remains about $\Gamma/2$ for all considered angles and magnetic fields, γ_e strongly varies with angle and magnetic field. With positive magnetic field along the z -direction, γ_e is higher at positive angles than that at negative angles. The emissivity in $B - \theta$ plane predicted from coupled mode theory for a thin film as shown in Fig. 4(f), shows good agreement with the measured emissivity in Fig. 4(d).

Using coupled mode theory, due to the approximate linear relationship of γ_e with respect to magnetic field and angle at positive magnetic field and $\theta \leq 60^\circ$ [Fig. 4(e)], and the approximately constant γ_i , emissivity is determined by the magnetic field and angle through γ_e . As a result, at large positive magnetic field and angle, due to the high γ_e and accordingly better matching between γ_e and γ_i , there is high emissivity. The coupled mode theory further suggests that emissivity can be maintained by maintaining the γ_e , by judiciously controlling the magnetic field and angle. Indeed, we observe that the measured emissivity can be largely maintained by adjusting magnetic field and angle with slopes of $-1.5^\circ/T$, $-5^\circ/T$, $-6.5^\circ/T$, and $-8^\circ/T$ corresponding to Figs. 4(a-d), respectively. Therefore, our work shows that magnetic field and angle can be combined to achieve novel control of emission.

To conclude, we demonstrated strong nonreciprocal thermal emission on a gradient epsilon-near-zero InGaAs multilayer, using a custom-designed angle-resolved magnetic thermal emission spectroscopy. The demonstrated nonreciprocity greatly exceeds those in the existing studies on direct measurements of nonreciprocal emission [29,30]. Significant nonreciprocal emission persists over broad spectral and angular ranges. Different from all prior studies on nonreciprocal emitters and absorbers [29-33], we transferred micrometer-scale-thick epitaxial gradient epsilon-near-zero structure to a foreign substrate, thus enabling its device integration for exploring nonreciprocal-based applications. It is noteworthy that due to the use of metal reflector enabled by epitaxial transfer, at wavelengths where the emission is largely reciprocal such as from 8.5-13 μm , our sample shows negligible parasitic reciprocal thermal emission (Fig. S3), which can be useful for application such as nonreciprocal heat flux control. In addition to nonreciprocal emission, we have achieved dramatic dynamic control of thermal emission by magnetic switching of thermal emission from one side to the other. The work also represents as a new approach to dynamic control of thermal radiation, in addition to electrical [34,35] and electrochemical mechanisms [36]. Our work highlights the dramatic opportunity of nonreciprocal control of

thermal emission and absorption. The achieved strong nonreciprocal emission over broad spectral and angular ranges can be useful for creating nonreciprocal-based applications such as heat flux control, energy conversion, and sensing [53].

Acknowledgments

L.Z. acknowledge support from National Science Foundation award no. 2238927, the Kaufman New Investigator Award through the Charles E. Kaufman Foundation - a supporting organization of the Pittsburgh Foundation, and Penn State Institute of Energy and the Environment (IEE) Seed Grant. We thank Dr. Bangzhi Liu in Penn State Materials Research Institute for support in scanning electron microscopy. We acknowledge use of Penn State Nanofabrication Lab and Materials Characterization Lab for fabricating and characterizing the sample.

References

- [1] G. Kirchhoff, *Annalen der Physik* **185**, 275 (1860).
- [2] M. Planck, *The Theory of Heat Radiation* (Dover Publications, 2013).
- [3] R. Siegel and J. R. Howell, *Thermal Radiation Heat Transfer, Fourth Edition* (Taylor & Francis, London, 2002).
- [4] S. H. Fan, *Joule* **1**, 264 (2017).
- [5] W. Li and S. Fan, *Opt. Express* **26**, 15995 (2018).
- [6] J. J. Greffet, R. Carminati, K. Joulain, J. P. Mulet, S. P. Mainguy, and Y. Chen, *Nature* **416**, 61 (2002).
- [7] X. Liu, T. Tyler, T. Starr, A. F. Starr, N. M. Jokerst, and W. J. Padilla, *Phys. Rev. Lett.* **107**, 045901, 045901 (2011).
- [8] J. Xu, J. Mandal, and A. P. Raman, *Science* **372**, 393 (2021).
- [9] M. A. Green, *Nano Letters* **12**, 5985 (2012).
- [10] Y. B. Park, B. Zhao, and S. H. Fan, *Nano Letters*, 448 (2022).
- [11] S. Buddhiraju, P. Santhanam, and S. H. Fan, *Proceedings of the National Academy of Sciences of the United States of America* **115**, E3609 (2018).
- [12] S. Jafari Ghalekohneh and B. Zhao, *Physical Review Applied* **18**, 034083 (2022).
- [13] W. Li, S. Buddhiraju, and S. Fan, *Light: Science & Applications* **9**, 68 (2020).
- [14] L. Zhu and S. Fan, *Phys. Rev. Lett.* **117**, 134303, 134303 (2016).
- [15] Y. Hadad, J. C. Soric, and A. Alu, *Proc. Natl. Acad. Sci. U. S. A.* **113**, 3471 (2016).
- [16] H. Ries, *Applied Physics B-Photophysics and Laser Chemistry* **32**, 153 (1983).
- [17] W. C. Snyder, Z. M. Wan, and X. W. Li, *Applied Optics* **37**, 3464 (1998).
- [18] D. A. B. Miller, L. X. Zhu, and S. H. Fan, *Proceedings of the National Academy of Sciences of the United States of America* **114**, 4336 (2017).
- [19] A. Davoyan and N. Engheta, *ACS PHOTONICS* **6**, 581 (2019).
- [20] Z. M. Zhang, X. H. Wu, and C. J. Fu, *Journal of Quantitative Spectroscopy & Radiative Transfer* **245**, 106904, 106904 (2020).
- [21] C. Khandekar, F. Khosravi, Z. Li, and Z. Jacob, *NEW JOURNAL OF PHYSICS* **22**, 123005, 123005 (2020).
- [22] S. Buddhiraju, W. Li, and S. H. Fan, *Phys. Rev. Lett.* **124**, 077402, 077402 (2020).

- [23] L. X. Zhu and S. H. Fan, *Physical Review B* **90**, 220301, 220301 (2014).
- [24] B. Zhao, Y. Shi, J. H. Wang, Z. X. Zha, N. Zhao, and S. H. Fan, *Optics Letters* **44**, 4203 (2019).
- [25] Z. Zhang and L. Zhu, *Physical Review Applied* **19**, 014013 (2023).
- [26] Y. Tsurimaki, X. Qian, S. Pajovic, F. Han, M. D. Li, and G. Chen, *Physical Review B* **101**, 165426, 165426 (2020).
- [27] B. Zhao, C. Guo, C. A. C. Garcia, P. Narang, and S. H. Fan, *Nano Letters* **20**, 1923 (2020).
- [28] S. Pajovic, Y. Tsurimaki, X. Qian, and G. Chen, *Physical Review B* **102**, 165417, 165417 (2020).
- [29] K. Shayegan, S. Biswas, B. Zhao, S. Fan, and H. Atwater, *NATURE PHOTONICS* **17**, 891 (2023).
- [30] K. Shayegan, J. Hwang, B. Zhao, A. Raman, and H. Atwater, *LIGHT-SCIENCE & APPLICATIONS* **13**, 176, 176 (2024).
- [31] M. Liu, S. Xia, W. Wan, J. Qin, H. Li, C. Zhao, L. Bi, and C.-W. Qiu, *Nature Materials* **22**, 1196 (2023).
- [32] K. J. Shayegan, B. Zhao, Y. Kim, S. Fan, and H. A. Atwater, *Science Advances* **8**, eabm4308 (2022).
- [33] L. Remer, E. Mohler, W. Grill, and B. Luthi, *Physical Review B* **30**, 3277 (1984).
- [34] T. Inoue, M. De Zoysa, T. Asano, and S. Noda, *Nature Materials* **13**, 928 (2014).
- [35] J. Park, J. Kang, X. Liu, S. Maddox, K. Tang, P. McIntyre, S. Bank, and M. Brongersma, *SCIENCE ADVANCES* **4**, eaat3163, eaat3163 (2018).
- [36] C. Sui *et al.*, *NATURE SUSTAINABILITY* **6**, 428 (2023).
- [37] See Supplemental Material [url] for fabrication of the sample, modeling of permittivity of InGaAs, measurement using the angle-resolved magnetic thermal emission spectroscopy, emissivity characterization of the high-emissivity coating, emissivity measurement of the InGaAs sample at room temperature, calculation of the modal decay rates in a single InGaAs layer, which includes Ref. [25] and Refs. [38-43].
- [38] T. Le, J. Pelouard, F. Charra, and S. Vassant, *OPTICAL MATERIALS EXPRESS* **12**, 2711 (2022).
- [39] T. P. Pearsall, *GaInAsP alloy semiconductors* (Wiley, New York, 1982).
- [40] N. B. Hannay and U. Colombo, *Electronic Materials* (Plenum Press, New York, 1973).
- [41] S. Paul, J. B. Roy, and P. K. Basu, *Journal of Applied Physics* **69**, 827 (1991).
- [42] M. Mikulicz, T. Smolka, M. Rygala, M. Badura, W. Kijaszek, A. Lozinska, M. Kamp, and M. Motyka, *PHYSICAL REVIEW APPLIED* **21**, 044001, 044001 (2024).
- [43] J. HAMEURY, J. Manara, and M. C. Arduini, https://www.euramet.org/research-innovation/search-research-projects/details/?tx_euramettcp_project%5Bproject%5D=1477 (2017).
- [44] S. Vassant, J. P. Hugonin, F. Marquier, and J. J. Greffet, *Optics Express* **20**, 23971 (2012).
- [45] D. J. Fan, T. Burger, S. McSherry, B. Lee, A. Lenert, and S. R. Forrest, *Nature* **586**, 237 (2020).
- [46] R. Mittapally, B. Lee, L. Zhu, A. Reihani, J. W. Lim, D. Fan, S. R. Forrest, P. Reddy, and E. Meyhofer, *Nature Communications* **12**, 4364, 4364 (2021).
- [47] O. Madelung, *Semiconductors : data handbook* (Springer, Heidelberg, 2004), 3rd edn.
- [48] H. B. G. Casimir, *Reviews of Modern Physics* **17**, 343 (1945).
- [49] C. Guo, B. Zhao, and S. H. Fan, *Physical Review X* **12**, 021023, 021023 (2022).
- [50] S. M. Rytov, A. P. Repeyev, Y. A. Kravtsov, and V. I. Tatarskii, *Principles of Statistical Radiophysics 4: Wave Propagation Through Random Media* (Springer Berlin Heidelberg, 1989).

- [51] L. X. Zhu, S. Sandhu, C. Otey, S. H. Fan, M. B. Sinclair, and T. S. Luk, *Appl. Phys. Lett.* **102**, 103104, 103104 (2013).
- [52] S. Fan, W. Suh, and J. Joannopoulos, *JOURNAL OF THE OPTICAL SOCIETY OF AMERICA A-OPTICS IMAGE SCIENCE AND VISION* **20**, 569 (2003).
- [53] Z. Zhang and L. Zhu, *PHYSICAL REVIEW APPLIED* **18**, 027001, 027001 (2022).